LETTERS
PUBLISHED ONLINE: 29 AUGUST 2016 | DOI: 10.1038/NPHYS3870

nature physics

A micrometre-sized heat engine operating between bacterial reservoirs

Sudeesh Krishnamurthy[1], Subho Ghosh[2], Dipankar Chatterji[2], Rajesh Ganapathy[3,4] and A. K. Sood[1,3]*

Artificial microscale heat engines are prototypical models to explore the mechanisms of energy transduction in a fluctuation-dominated regime[1,2]. The heat engines realized so far on this scale have operated between thermal reservoirs, such that stochastic thermodynamics provides a precise framework for quantifying their performance[3–6]. It remains to be seen whether these concepts readily carry over to situations where the reservoirs are out of equilibrium[7], a scenario of particular importance to the functioning of synthetic[8,9] and biological[10] microscale engines and motors. Here, we experimentally realize a micrometre-sized active Stirling engine by periodically cycling a colloidal particle in a time-varying optical potential across bacterial baths characterized by different degrees of activity. We find that the displacement statistics of the trapped particle becomes increasingly non-Gaussian with activity and contributes substantially to the overall power output and the efficiency. Remarkably, even for engines with the same energy input, differences in non-Gaussianity of reservoir noise results in distinct performances. At high activities, the efficiency of our engines surpasses the equilibrium saturation limit of Stirling efficiency, the maximum efficiency of a Stirling engine where the ratio of cold to hot reservoir temperatures is vanishingly small. Our experiments provide fundamental insights into the functioning of micromotors and engines operating out of equilibrium.

In a seminal experiment, Blickle and Bechinger[3] devised a micrometre-sized Stirling heat engine that was driven by fluctuations from an equilibrium thermal reservoir, while being subject to time-dependent potentials in an optical trap. Like its macroscopic counterpart, the mean quasistatic efficiency of such an engine (approximately 14% for a colloidal bead in water) is given by $\mathcal{E}_\infty = \mathcal{E}_c[1+\mathcal{E}_c/\ln[(k_{max}/k_{min})]]^{-1}$. Here, $\mathcal{E}_c = 1-(T_C/T_H)$ is the Carnot efficiency, T_C and T_H are the cold and hot reservoir temperatures, respectively, and the ratio of trap stiffnesses (k_{max}/k_{min}) is analogous to the compression ratio of a macroscopic engine. By imposing an external source of noise on the trapped colloidal particle, corresponding to an effective T_H of nearly 3,000 K (ref. 11), and implementing the microscopic equivalent of an adiabatic process, a Brownian Carnot engine with higher power output and efficiency was later realized[4]. Although strategies for harnessing the work done by these microscale heat engines have not yet been devised, these studies underscore the feasibility of using a colloidal particle as the working substance of a heat engine to elucidate the role of fluctuations on its performance. In microscale heat engines investigated hitherto, noise fluctuations associated with the reservoirs decorrelate on a timescale that is much smaller than that associated with the working substance—the Brownian time of the colloidal bead. Owing to this separation of timescales, particle dynamics in such reservoirs follow Gaussian statistics and equilibrium stochastic thermodynamics can be readily applied. However, in a bath of active particles—a canonical athermal reservoir, noise fluctuations can remain temporally correlated for substantially longer[12]. This results in the breakdown of the fluctuation–dissipation theorem[13,14] and, as a consequence, particle dynamics in active reservoirs follow non-Gaussian statistics over suitable time and length scales[15,16]. Importantly, while stochastic thermodynamics models show that between athermal reservoirs with identical noise intensities (that is, temperatures), heat flow is still possible due to a difference in the non-Gaussianity of their noises[17,18], whether work can also be extracted remains unclear. Moving outside the realm of stochastic thermodynamics, quantum analogues of classical heat engines[19–22] coupled to athermal reservoirs are predicted to operate at efficiencies that surpass the equilibrium Carnot efficiency[23,24]. In light of these theoretical advances, a natural step forward would be the experimental realization of microscale heat engines that exploit features unique to athermal reservoirs for extracting work.

Here we designed, constructed and quantified the working of an active heat engine. A 5 μm colloidal bead, held in a harmonic optical trap, in a suspension of motile bacteria—*Bacillus licheniformis*—acts as the working substance. The time-dependent variations in laser intensity, that is, trap strength, mimic the role of the piston of a macroscopic engine. A key advantage of utilizing a bacterial reservoir is that bacterial metabolism and the corresponding activity are strongly sensitive to the bath temperature[25,26]. We exploit this behaviour and periodically create conditions of high and low activity, thus imitating passive reservoirs with a temperature difference (see Methods and Supplementary Text and Supplementary Figs 1 and 2). The bacterial activity depends on a host of physico-chemical parameters and was found to be exclusive to each experiment. This allowed us to access reservoirs with different activities, while keeping the bacterial number density constant. We parametrized bacterial activity by an active temperature, $k_B T_{act} = (1/2)k_x\langle x^2\rangle + (1/2)k_y\langle y^2\rangle$ (refs 16,27). Here, k_x, x and k_y, y are trap stiffness and the displacement of the bead from the trap centre, respectively, along the x and y directions. The engine is driven by fluctuations arising from the differences in bacterial activity across the reservoirs, ΔT_{act}, and we execute the microscopic equivalent of a Stirling cycle.

The active Stirling cycle executed by the engine, as outlined in Fig. 1, is analogous to its passive counterpart[3], except here, the activity of the bath is maintained constant during the

[1]Department of Physics, Indian Institute of Science, Bangalore - 560012, India. [2]Molecular Biophysics Unit, Indian Institute of Science, Bangalore - 560012, India. [3]International Centre for Materials Science, Jawaharlal Nehru Centre for Advanced Scientific Research, Jakkur, Bangalore - 560064, India. [4]Sheikh Saqr Laboratory, Jawaharlal Nehru Centre for Advanced Scientific Research, Jakkur, Bangalore - 560064, India.
*e-mail: asood@physics.iisc.ernet.in

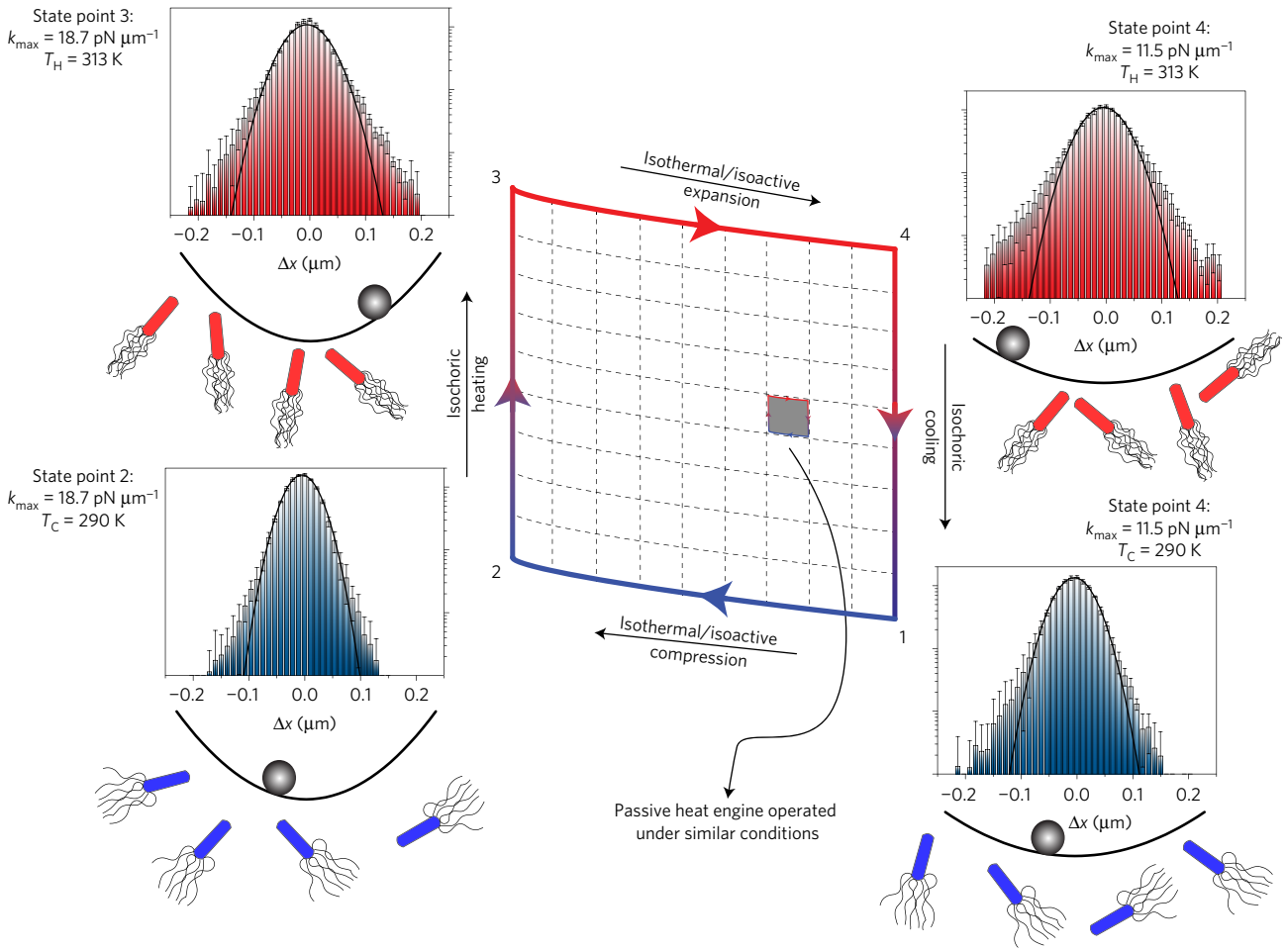

Figure 1 | Micrometre active Stirling engine. A Stirling cycle consists of isothermal compression (1 → 2) and expansion (3 → 4) steps at temperatures T_C and T_H, respectively, connected by isochores 2 → 3 and 4 → 1. In the active Stirling engine, for large activities, a substantial contribution to the total work stems from bacterial activity, and the isotherms can be effectively replaced by isoactivity lines. Increasing (decreasing) the trap stiffness decreases (increases) the phase space volume available to the colloidal particle and mimics a compression (expansion) stroke of a macroscopic Stirling engine. $P(\Delta x)$ at state points 3 and 4 are substantially more non-Gaussian than at state points 1 and 2 due to increased bacterial activity. The black lines represent Gaussian fits. The error bars represent standard error of the mean (SEM) from four independent realizations of the engine with different bacterial samples of approximately the same ΔT_{act}. The area of the large(small) Stirling cycle represents the average work done by the active(passive) engine as it executes one Stirling cycle.

isothermal processes (1 → 2 & 3 → 4), while k_x and k_y are linearly increased(decreased) to mimic compression(expansion) of the system. The isochoric processes (2 → 3 & 4 → 1) now correspond to changing the activity while maintaining k_x and k_y constant (see Methods). The compression/expansion of the trap as well as the change in activity is captured by the probability distributions in the x-position, $P(\Delta x)$, of the colloidal bead. Owing to non-equilibrium fluctuations, $P(\Delta x)$ shows strong non-Gaussian behaviour. The position of the colloidal bead represents the state of the system as the cyclic process described in Fig. 1 is steadily executed and thermodynamic quantities were computed using the framework of stochastic thermodynamics[6,28]. Since fluctuations in our system follow non-Gaussian statistics, T_{act} cannot be used to define thermodynamic quantities. As per the definition, T_{act} is the temperature of an equilibrium reservoir with the same average potential energy $\langle U \rangle$ as the trapped bead in our bacterial reservoir. Thus, the equilibrium reservoir at T_{act} and our bacterial reservoir transfer the same amount of heat during an isochoric process.

We first compared the performance of an active engine with a passive one (see Supplementary Movies 1 and 2). For the highest activity accessible in our experiments, the work done per cycle, W_{cycle}, of the active engine, represented by the area of the larger Stirling cycle in Fig. 1, is about two orders of magnitude larger than that of the passive engine (see Supplementary Figs 5 and 6). A comparison of heat engines is possible only in the quasistatic limit (cycle duration $\tau \to \infty$) or at peak power output (see Methods). Here we operate our engines in the quasistatic limit. In the quasistatic limit, the instantaneous $P(\Delta x)$ of the colloidal particle should mimic the closing (1 → 2) and opening (3 → 4) of the optical trap. This implies, $k(t_1)\langle \Delta x^2(t_1) \rangle = k(t_2)\langle \Delta x^2(t_2) \rangle = k_B T$, where t_1 and t_2 denote any two time instances along the isotherms. Thus, the $P(\Delta x)$ values (determined over suitably small time bins), when appropriately scaled, should collapse, and this is indeed observed for $\tau = 22$ s (Fig. 2a) (see also Supplementary Fig. 7). The engines are thus operating in the quasistatic limit, which enables a direct comparison of engine performance across activities.

In Fig. 2b, we show the cumulative work done, in units of $k_B T_C (T_C = 290\,\mathrm{K})$, at the end of each Stirling cycle by the passive engine (filled symbols) and the active engine (open symbols), for various values of ΔT_{act}. The error bars for each ΔT_{act} are obtained from multiple experimental realizations and represent the standard error of the mean (SEM) (see Supplementary Fig. 5). Since the work is cumulative, so is the error. The slopes of the trajectories are negative, and work is done by the engine on the surroundings.

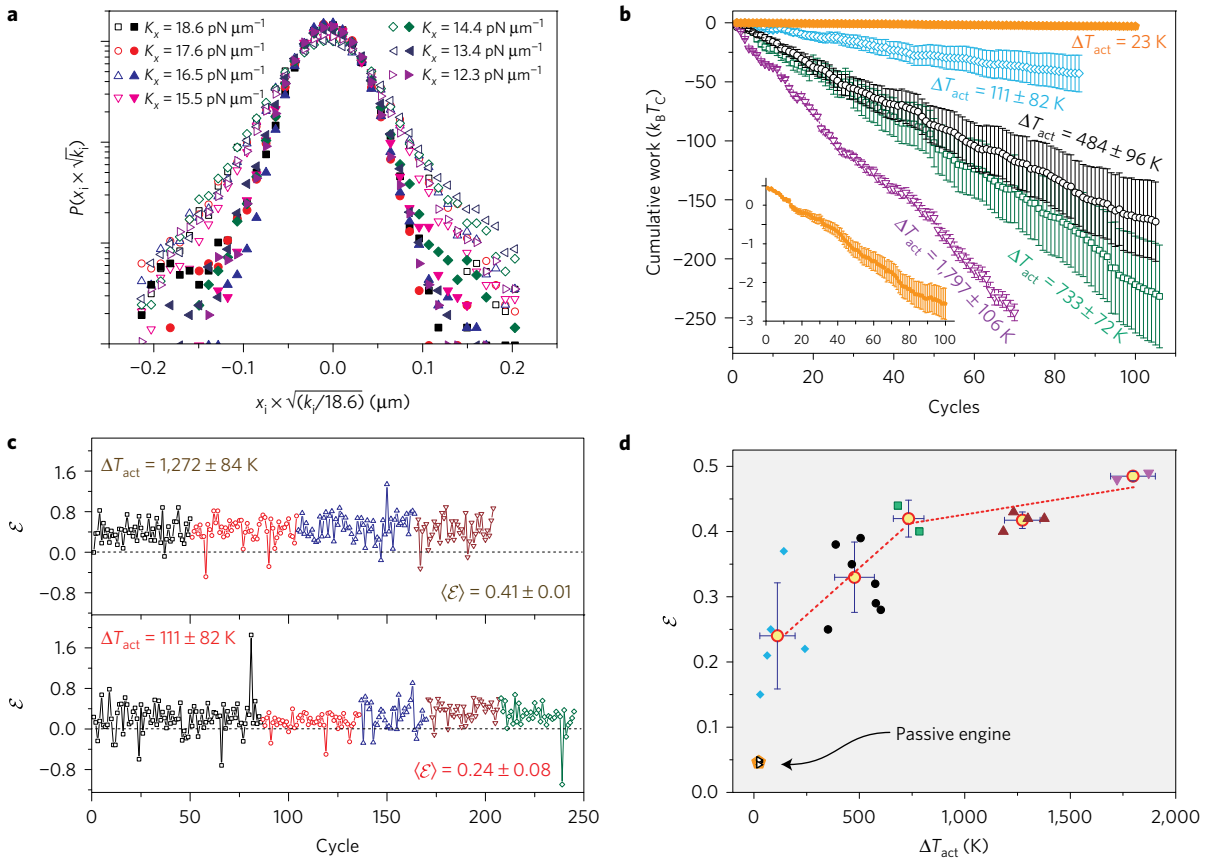

Figure 2 | Comparison of active engines at different activities. a, Scaled $P(\Delta x)$ values at different instances along the isothermal expansion stroke (3→4) for two different activities. $\Delta T_{act} = 63$ K (filled symbols) and $\Delta T_{act} = 1{,}299$ K (open symbols). **b**, Cumulative work done by active (open symbols) and passive (filled symbols) engine for different values of ΔT_{act}. The error bars represent standard error of the mean obtained from multiple realizations for approximately the same ΔT_{act} and are cumulative. Inset to **b** shows work done by the passive engine on a scale where fluctuations are visible. **c**, Fluctuations in efficiency of the active engine as the Stirling cycle is continuously executed for two values of ΔT_{act}. The different colours and symbols represent individual realizations for each ΔT_{act}. **d**, Average efficiency of the active engine (red circles) and the passive engine (orange pentagon) estimated from multiple experimental realizations for approximately the same ΔT_{act}. The x and y-error bars correspond to SEM of ΔT_{act} and $\mathcal{E}$, respectively. The symbol colour and shape corresponds to individual realizations that have nearly the same ΔT_{act}.

With increasing activity, the cumulative work steadily increases (Fig. 2b) and, at the highest activities investigated, ΔT_{act} is in excess of 1,200 K. Such enormous differences in reservoir temperatures are impossible to mimic in passive microengines without an external source of noise[11]. W_{cycle} is a fluctuating quantity due to the stochastic nature of the engine, and so is the efficiency, $\mathcal{E}_{cycle}$. Figure 2c shows these fluctuations for multiple realizations of active engines corresponding to $\Delta T_{act} = 1{,}272 \pm 84$ K (top panel) and 111 ± 82 K (bottom panel), respectively. In Fig. 2d, the open triangles and filled symbols represent $\langle \mathcal{E}_{cycle} \rangle$ for individual realizations of the passive and active heat engine, respectively. The red circles denote efficiency $\mathcal{E}$ averaged over active engines with nearly the same ΔT_{act} (shown by similar symbols). Most remarkably, at the highest activity, $\mathcal{E}$ of the bacterial engine is almost an order of magnitude larger than its passive counterpart, and is only a factor of two smaller than biological motors[10]. Experiments carried out at a different k_{max} and k_{min}, but with same (k_{max}/k_{min}), showed similar trends in both work and efficiency (see Supplementary Information).

For equilibrium engines operating in the quasistatic limit, the work done per cycle is given by $W_q = 2k_B T_C[1 - (T_H/T_C)] \ln\sqrt{(k_{max}/k_{min})}$. W_q and $\mathcal{E}_q$ for the passive engine, represented by open inverted triangles in Fig. 3a,b, closely match the experimental values (filled pentagons) and reaffirm that we are operating the engine in the quasistatic limit. Turning our attention to the active engines, we find that while W increases steadily with ΔT_{act} (Fig. 3a), $\mathcal{E}$ increases and then shows a tendency to saturate at high ΔT_{act} (Fig. 3b, and Supplementary Fig. 5). Such a behaviour is typical of an equilibrium Stirling engine, where the quasistatic efficiency saturates to $\mathcal{E}_{sat} = (1 + 1/\ln(k_{max}/k_{min}))^{-1}$ as $T_C/T_H \to 0$, represented by the solid horizontal line in Fig. 3b. The experimentally determined efficiencies surpass this limit, suggesting a failure of the equilibrium description in evaluating $\mathcal{E}_{sat}$ for the active engines.

To understand the origin(s) of such high $\mathcal{P}$ and $\mathcal{E}$ of our active engines, we carefully examined the fluctuations of the trapped colloidal particle in the active reservoirs. $P(\Delta x)$ in the hot(cold) reservoir for $\Delta T_{act} = 1{,}272 \pm 84$ K is shown by the red(blue) histogram in Fig. 3c. The green line represents a Gaussian fit to $P(\Delta x)$. To isolate the contributions from Gaussian fluctuations to the total W and $\mathcal{E}$, we simulated Stirling cycles by drawing particle displacements at random from the Gaussian region alone (green shaded area). A cumulative sum of these displacements yielded particle trajectories using which, the work done, W^G and the efficiency, $\mathcal{E}^G$ were calculated (see Supplementary Information). For such a Gaussian engine, an effective temperature T_{eff} can be precisely defined and $\Delta T_{eff} < \Delta T_{act}$ (top x-axis in Fig. 3a,b) since we have chosen only the low-energy contributions to $\langle U \rangle$. $\langle W^G \rangle$ and $\langle \mathcal{E}^G \rangle$ for the simulated Gaussian engine are shown as green circles in Fig. 3a and b, respectively. Strikingly, at the highest activity, 57% of total W and 55% of the total $\mathcal{E}$ are due to non-Gaussian fluctuations. In fact, these fluctuations account for ~59% of the potential energy

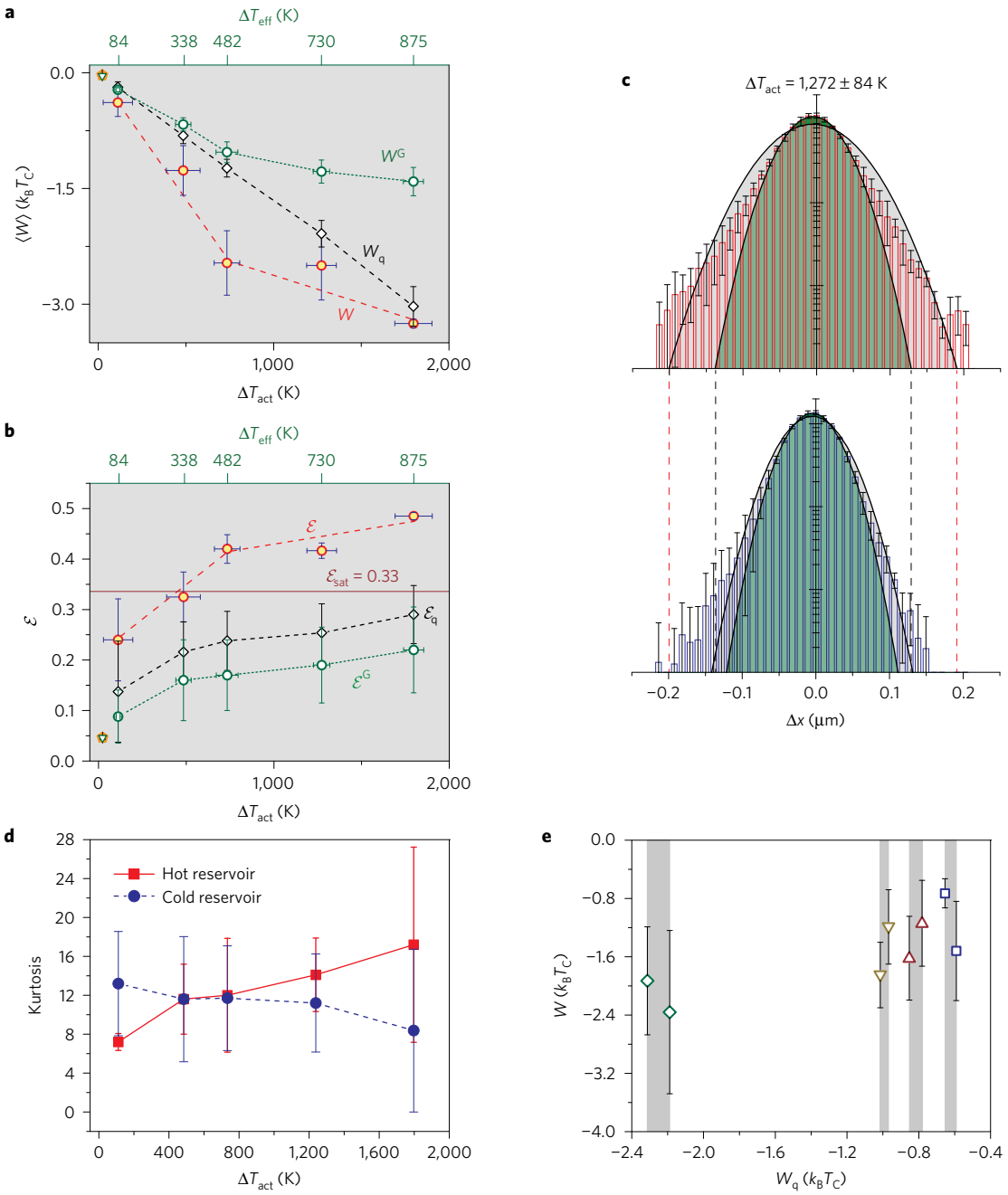

Figure 3 | Elucidating the origins of active engine performance. a,**b**, Work done (**a**) and efficiency (**b**) for the experimental and simulated engines, respectively. The red lines are only a guide to the eye. Experimental and calculated W and $\mathcal{E}$ for passive engines are represented by a filled pentagon and open inverted triangle, respectively. Solid circles represent an experimental active engine, open circles represent a simulated Gaussian engine and diamonds represents the quasistatic Stirling engine. The efficiency of passive engines saturates for $T_C/T_H \to 0$ at $\mathcal{E}_{sat}$ represented by the brown line in **b**. **c**, Experimental $P(\Delta x)$ values at trap stiffness, $k = k_{min}$, in the hot (red bars) and cold (blue bars) reservoirs for $\Delta T_{act} = 1{,}272 \pm 84$ K. The green line represents the Gaussian fit to the data and the fluctuations in the green shaded region alone contribute to W^G and $\mathcal{E}^G$ (green circles in **a** and **b**). The black line represents a Gaussian engine with the same variance as the experimental active engine and is an overlay. Fluctuations within the grey shaded area contribute to W_q and $\mathcal{E}_q$. **d**, Average kurtosis of $P(\Delta x)$ for hot(red squares) and cold(blue circles) reservoirs for different values of ΔT_{act}. In **a**–**d**, the x and y-error bars correspond to the SEM of the respective quantities obtained from multiple realizations. **e**, Work, W, done by active engines versus work done by a Gaussian engine with the same variance, W_q. Points that lie within the grey bars correspond to engines with approximately the same ΔT_{act} and hence the same W_q. The average experimental work, however, differs due to differences in non-Gaussian statistics. The error bars represent the standard deviation within an individual realization.

difference between the hot and cold reservoirs (Fig. 3c), explaining their large contribution to W (see Methods).

We can further compare the experimental active engine with a passive engine operating between equilibrium reservoirs at the same $\langle \Delta U \rangle$, that is, the same ΔT_{act}. The solid black curve in Fig. 3c represents a Gaussian with width equal to the variance of $P(\Delta x)$ of the active engine. The black diamonds in Fig. 3a and b show W_q and $\mathcal{E}_q$, respectively, for a quasistatic equilibrium Stirling engine operating under such conditions. W_q and $\mathcal{E}_q$ continue to remain smaller than W and $\mathcal{E}$ of the corresponding active engine. For

$\Delta T_{act} = 1{,}272 \pm 84$ K, 20% of the contribution to the total work done stems from a few large displacements seen outside of the grey shaded area of the Fig. 3c. These fluctuations comprise about 21% of the difference in U between the $P(\Delta x)$ of the hot and cold reservoirs. For intermediate activities, these large displacements contribute as much as 50% to the total work. We quantified the non-Gaussianity of the distributions, by examining the kurtosis for various bacterial activities (Fig. 3d). The squares and circles in Fig. 3d represent the kurtosis of $P(\Delta x)$ at state points 4 and 1 of the Stirling cycle (see Fig. 1), respectively. The observed increase in the difference in kurtosis between the hot and cold reservoirs confirms that the superior performance of the active engine vis-á-vis equilibrium/Gaussian engines stems entirely from non-Gaussian statistics. Further, while the experimental errors in estimating $\langle W_{cycle} \rangle$ and $\langle \mathcal{E}_{cycle} \rangle$ for passive engines is small, differences in kurtosis for individual realizations with similar ΔT_{act} result in a larger spread in these quantities for active engines. Most remarkably, even for engines with the same ΔT_{act}, that is, the same W_q, the experimental work done is different (Fig. 3e). This implies that work can be extracted due to differences in the statistics alone even when the noise intensities of the reservoirs remain the same.

Collectively, our results show that active engines significantly outperform passive engines, which are bound by the laws of thermodynamics. While one would naively interpret such a result as an outcome of continuous energy input, our experiments demonstrate that the superior performance of active engines arises from access to temporal regimes dominated by non-Gaussian statistics. Our results show that, despite being rare, the non-Gaussian fluctuations[15,16] in position and hence velocity (that is, departure from the equipartition theorem) contribute significantly to the performance and should be explicitly taken into account in future theories. Given that biological motors are known to operate under isothermal conditions[10], it is tempting to speculate if the mechanisms expounded here are also the source of their observed high efficiencies. In view of the recent advances in the fabrication of synthetic self-propelled colloids[29] that can be rendered active by light fields, for example, active reservoirs should be an integral part of the design of future microscopic heat engines that can potentially power microscale and nanoscale electro-mechanical devices.

Methods

Methods, including statements of data availability and any associated accession codes and references, are available in the online version of this paper.

Received 11 January 2016; accepted 29 July 2016; published online 29 August 2016

References

1. Horowitz, J. M. & Parrando, J. M. R. A Stirling effort. *Nat. Phys.* **8,** 108–109 (2012).
2. Hangii, P. & Marchesoni, F. Artificial Brownian motors: controlling transport on the nanoscale. *Rev. Mod. Phys.* **81,** 387–442 (2009).
3. Blickle, V. & Bechinger, C. Realization of micrometer sized stochastic heat engine. *Nat. Phys.* **8,** 143–146 (2012).
4. Martinez, I. A. *et al*. Brownian Carnot engine. *Nat. Phys.* **12,** 67–70 (2016).
5. Sekimoto, K. Langevin equation and thermodynamics. *Prog. Theor. Phys. Suppl.* **130,** 17–27 (1998).
6. Seifert, U. Stochastic thermodynamics, fluctuation theorems and molecular machines. *Rep. Prog. Phys.* **75,** 126001 (2012).
7. Das, S., Narayan, O. & Ramaswamy, S. Ratchet for energy transport between identical reservoirs. *Phys. Rev. E* **66,** 050103 (2002).
8. Browne, W. R. & Feringa, B. L. Making molecular machines work. *Nat. Nanotech.* **1,** 25–35 (2006).
9. Balzani, V. *et al*. Artificial molecular machines. *Angew. Chem. Int. Ed.* **39,** 3348–3391 (2000).
10. Howard, J. *Mechanics of Motor Proteins and the Cytoskeleton* (Sinauer Associates Sunderland, 2001).
11. Martinez, I. A., Roldan, E., Parrando, J. M. R. & Petrov, D. Effective heating to several thousand kelvins of an optically trapped sphere in a liquid. *Phys. Rev. E* **87,** 032159 (2013).
12. Soni, G. V., Jaffar Ali, B. M., Hatwalne, Y. & Shivshankar, G. V. Single particle tracking of correlated bacterial dynamics. *Biophys. J.* **84,** 2634–2637 (2003).
13. Wu, X. L. & Libchaber, A. Particle diffusion in a quasi-two-dimensional bacterial bath. *Phys. Rev. Lett.* **84,** 3017 (2001).
14. Chen, D. T. N. *et al*. Fluctuations and rheology in active bacterial suspensions. *Phys. Rev. Lett.* **99,** 148302 (2007).
15. Tailleur, J. & Cates, M. E. Sedimentation, trapping, and rectification of dilute bacteria. *Euro. Phys. Lett.* **86,** 60002 (2008).
16. Maggi, C. *et al*. Generalized energy equipartition in harmonic oscillators driven by active baths. *Phys. Rev. Lett.* **113,** 238303 (2014).
17. Kanazawa, K., Sagawa, T. & Hayakawa, H. Stochastic energetics of non-Gaussian processes. *Phys. Rev. Lett.* **108,** 210601 (2012).
18. Kanazawa, K., Sagawa, T. & Hayakawa, H. Heat conduction induced by non-Gaussian athermal fluctuations. *Phys. Rev. E* **87,** 052124 (2013).
19. Scully, M. O., Zubairy, S. M., Agarwal, G. S. & Walther, H. Extracting work from a single heat bath via vanishing quantum coherence. *Science* **299,** 862–864 (2003).
20. Koski, J. V., Maisi, V. F., Pekola, J. P. & Averin, D. V. Experimental realization of a Szilard engine with a single electron. *Proc. Natl Acad. Sci. USA* **111,** 13786–13789 (2014).
21. Abah, O. *et al*. Single-ion heat engine at maximum power. *Phys. Rev. Lett.* **109,** 203006 (2012).
22. Dechant, A., Kiesel, N. & Lutz, E. All-optical nanomechanical heat engine. *Phys. Rev. Lett.* **114,** 183602 (2015).
23. Lutz, E. & Abah, O. Efficiency of heat engines coupled to non-equilibrium reservoirs. *Euro. Phys. Lett.* **106,** 20001 (2014).
24. Rossnagel, J., Abah, O., Schmidt-Kaler, F., Singer, K. & Lutz, E. Nanoscale heat engine beyond Carnot limit. *Phys. Rev. Lett.* **112,** 030602 (2014).
25. Shneider, W. R. Jr & Doetsch, R. N. Temperature effects on bacterial movement. *Appl. Environ. Microbiol.* **34,** 695–700 (1977).
26. Lewis, P. & Ford, R. M. Temperature-sensitive motility of *Sulfolobus acidocaldarius* influences population distribution in extreme environments. *J. Bacteriol.* **181,** 4020–4025 (1999).
27. Palacci, J., Cottin-Bizonne, C., Ybert, C. & Bocquet, L. Sedimentation and effective temperature of active colloidal suspensions. *Phys. Rev. Lett.* **105,** 088304 (2010).
28. Blickle, V., Speck, T., Helden, L., Seifert, U. & Bechinger, C. Thermodynamics of a colloidal particle in a time-dependent nonharmonic potential. *Phys. Rev. Lett.* **96,** 070603 (2006).
29. Aranson, I. S. Active colloids. *Phys. Uspekhi.* **56,** 79–92 (2013).

Acknowledgements

We thank U. Seifert for illuminating discussions and S. Ramaswamy and S. Gokhale for critical comments on our manuscript. S.K. thanks the J C Bose Fellowship of the Department of Science and Technology (DST) for fellowship support. S.G. thanks the Council of Scientific and Industrial Research for fellowship support. D.C. thanks the Department of Biotechnology for financial support. A.K.S. thanks the J C Bose Fellowship of the DST, India for support. R.G. thanks the ICMS and SSL, JNCASR for financial support.

Author contributions

S.K., R.G. and A.K.S. conceived the project. S.K. designed and performed the experiments. S.G. and D.C. contributed towards handling and complete characterization of the bacteria. S.K., R.G. and A.K.S. analysed results. S.K., R.G. and A.K.S. wrote the paper with inputs from D.C. and S.G.

Additional information

Supplementary information is available in the online version of the paper. Reprints and permissions information is available online at www.nature.com/reprints. Correspondence and requests for materials should be addressed to A.K.S.

Competing financial interests

The authors declare no competing financial interests.

Methods

Bacterial strain and growth condition. *Bacillus licheniformis* (Weigmann 1898) Chester 1901 (also known as *B. licheniformis* ATCC 14580) was bought from Microbial Culture Collection at the National Centre for Cell Science, Pune, India (Catalog No.-MCC 2047). Bacteria were grown in Tartoff–Hobbs Hiveg broth (Himedia) at 37 °C with vigorous shaking. The suspension of bacteria was aliquoted for experiment at the sixth hour of growth in 5 ml of Tartoff–Hobbs Hiveg broth.

Laser trapping and particle position determination. The crosslinked poly(styrene/divinylbenzene) (P[S/DVB]) particles of 5 μm were obtained from Bangslabs, USA. The particles were trapped in a optical trap obtained by tightly focusing an infrared laser beam (NdYVO4 laser of wavelength 1,064 nm) with a ×100 (1.4 NA) objective mounted on a Carl Zeiss Axiovert Microscope. An extremely low power aligned red laser (Thorlabs ML101J8 Diode laser of wavelength 632 nm controlled using a Thorlabs TCLDM9 temperature-controlled laser diode module) is switched on during the isochoric process and is used as a marker to define the end points of the process with an accuracy within the limits of our temporal resolution (see Supplementary Movies 1 and 2). T_{bath} is tuned by flowing a heat exchanging fluid, in this case water, in a channel adjacent to the bacterial reservoir. The bacterial reservoir and the heat exchanging fluid are separated by a #1 (100 μm thick) glass coverslip for quick equilibration. Particles were imaged using a Basler Ace 180 kc colour camera at 500 frames/s. Only the green slice of the RGB image was considered so as to eliminate the influence of the red laser(632 nm) on the particle position. The particle was tracked to sub-pixel resolution using the tracking codes by R. Parthasarathy[30]. The particle positions could be determined with an accuracy of 10 nm.

Active Stirling cycle. A typical cycle executed by the engine is outlined in Fig. 1. The process starts at state point 1 where $T_C = 290$ K and trap stiffness $k = k_{min} = 11.5\,\mathrm{pN\,\mu m^{-1}}$ (see Supplementary Fig. 4). Bacteria in this state are sluggish but still active. The probability distribution of displacements in the x-position, $P(\Delta x)$, of the colloidal bead corresponding to this state point is also shown. The error bars in the histograms represent standard error of the mean and are obtained from multiple realizations of the Stirling cycle for approximately the same ΔT_{act}. The black line is a Gaussian fit to the data and points outside the fit represent non-Gaussian displacements. The trap stiffness k is increased linearly to $k_{max} = 18.7\,\mathrm{pN\,\mu m^{-1}}$, analogous to a macroscopic isothermal compression, and the system reaches the state point 2. The increase in k results in a narrower $P(\Delta x)$. The bath temperature is increased to $T_H = 313$ K at $k = k_{max}$ and the system reaches state point 3. A substantial increase in the width of $P(\Delta x)$ due to enhanced bacterial activity during the isochoric heating is clearly evident (Fig. 1). k is decreased linearly to k_{min}, analogous to a macroscopic isothermal expansion, and the system reaches state point 4. Finally, by isochoric cooling to T_C, keeping $k = k_{min}$, the cycle returns back to state point 1. T_C and T_H are kept the same for the passive (no bacteria present) as well as the active engine for all activities investigated. The isothermal processes were executed in 7 s and isochoric processes in 4 s, and the time taken to complete one Stirling cycle, $\tau = 22$ s, was held constant (see Supplementary Information and Supplementary Fig. 4). The position of the colloidal bead represents the state of the system as the cyclic process described in Fig. 1 is steadily executed.

Quantifying the performance of Active Stirling engines. Thermodynamic quantities were computed from particle trajectories using the framework of stochastic thermodynamics[6,28]. The work done by the engine is $W = \int (\partial U/\partial t)\mathrm{d}t$, where $U(x,t) = (1/2)k(t)x(t)^2$, with $x(t)$ being the displacement of the bead from the trap centre at time t. In this sign convention the work done, W, by (on) the system on(by) the surroundings is negative(positive). W is non-zero during the isothermal processes ($1 \to 2$ and $3 \to 4$) and zero in the isochoric processes ($2 \to 3$ and $4 \to 1$). Heat transferred, Q, by the reservoir in the isothermal processes can be calculated using an energy balance reminiscent of the first law of thermodynamics, $DU = Q - W$, despite Q and W being fluctuating quantities[28]. The energy balance is observed to be true for our active engines as well (see discussion following equation 6 of Supplementary Information). In the isothermal processes $DU = 0$ and $Q = W$. Heat transferred during the isochoric processes is calculated using $Q = -\int (\partial U/\partial x)\dot{x}\mathrm{d}t$ and, for constant k, results in a path-independent form for $Q = -(k/2)\left[x^2\right]_0^t$. The efficiency of the engine is defined as $\mathcal{E}_{cycle} = W_{cycle}/Q_h$, where Q_h is the heat transferred in the isothermal expansion $3 \to 4$ and W_{cycle} is the work done at the end of the Stirling cycle. Since fluctuations in our system follow non-Gaussian statistics, T_{act} cannot be used to define thermodynamic quantities. As per the definition, T_{act} is the temperature of an equilibrium reservoir with the same average potential energy $\langle U \rangle$ as the trapped bead in our bacterial reservoir. Thus, the equilibrium reservoir at T_{act} and our bacterial reservoir transfer the same amount of heat during an isochoric process.

$\mathcal{P}$ for a heat engine is a non-monotonic function of τ. As $\tau \to 0$, a substantial amount of heat drawn from the hot reservoir is lost towards irreversible work, W_{irr}, and $\mathcal{P}$ is small since W is small. For large cycle durations ($\tau \to \infty$), that is, the quasistatic limit, while both W_{irr} and $\mathcal{P} \to 0$, $\mathcal{E}$ reaches its maximum as the heat drawn during the isotherms is completely converted to work. The performance of engines in this limit is described by equilibrium stochastic thermodynamics. For intermediate τ, however, a trade-off between W_{irr} and τ results in a maximum in $\mathcal{P}$ (refs 31,32). Thus, a comparison across engines is possible only at maximum $\mathcal{P}$ or in the quasistatic limit (maximum $\mathcal{E}$), where the nature of irreversibility is well understood.

Origin of non-Gaussian fluctuations. The non-Gaussian fluctuations of particles in active reservoirs is a result of the underlying bacterial motility. It was recently shown that a colloidal particle diffusing in an active bath in the absence of any confining potential shows super-diffusive behaviour for times smaller than a characteristic time, τ_c (refs 13,33). In our experiment, $\tau_c \sim 1s$ (see Supplementary Information and Supplementary Fig. 9), while the timescale over which the particle experiences the optical trap is of the order of 10 ms. Further, exact solutions[15] to the Langevin equation for a self-propelled particle in a harmonic trap suggests that the shape of $P(\Delta x)$ is determined by parameter $a = (2\mu k\tau_c)^{-1}$, where μ is the mobility of the particle. $P(\Delta x)$ shows Gaussian behaviour as $a \sim 1$, and becomes increasingly non-Gaussian in the limit $a \ll 1$. In our experiment, $a \sim 10^{-4}$ and $P(\Delta x)$ is strongly non-Gaussian. The Gaussian behaviour is recovered in the macroscopic limit of smoothly varying potentials ($k \to 0$) or large particle diameters ($\mu \to 0$). Thus, our observations arise as a consequence of operating the engine in a spatial and temporal regime that precedes the onset of an effective equilibrium.

Data availability. The data that support the plots within this paper and other findings of this study are available from the corresponding author upon request.

References

30. Parthasarathy, R. Rapid, accurate particle tracking by calculation of radial symmetry centers. *Nat. Methods* **9,** 724–726 (2012).
31. Schmiedl, T. & Seifert, U. Efficiency at maximum power: an analytically solvable model for stochastic heat engines. *Euro. Phys. Lett.* **81,** 20003 (2008).
32. Curzon, F. L. & Ahlborn, B. Efficiency of a Carnot engine at maximum power output. *Am. J. Phys.* **43,** 22–24 (1975).
33. Hatwalne, Y., Ramaswamy, S., Rao, M. & Simha, R. A. Rheology of active-particle suspensions. *Phys. Rev. Lett.* **92,** 118101 (2004).